PHYSICAL REVIEW B **84**, 060504(R) (2011)

Topological phases and surface flat bands in superconductors without inversion symmetry

Andreas P. Schnyder[1] and Shinsei Ryu[2]
[1]*Max-Planck-Institut für Festkörperforschung, Heisenbergstrasse 1, D-70569 Stuttgart, Germany*
[2]*Department of Physics, University of California, Berkeley, California 94720, USA*
(Received 11 July 2011; published 11 August 2011)

We examine different topological phases in three-dimensional noncentrosymmetric superconductors with time-reversal symmetry by using three different types of topological invariants. Due to the bulk boundary correspondence, a nonzero value of any of these topological numbers indicates the appearance of zero-energy Andreev surface states. We find that some of these boundary modes in nodal superconducting phases are dispersionless, i.e., they form a topologically protected flat band. The region where the zero-energy flat band appears in the surface Brillouin zone is determined by the projection of the nodal lines in the bulk onto the surface. These dispersionless Andreev surface bound states have many observable consequences, in particular, a zero-bias conductance peak in tunneling measurements. We also find that in the gapless phase there appear Majorana surface modes at time-reversal invariant momenta which are protected by a $\mathbb{Z}_2$ topological invariant.

DOI: 10.1103/PhysRevB.84.060504 PACS number(s): 73.43.−f, 03.65.Vf, 73.20.−r, 74.55.+v

The hallmark of topological insulators and superconductors (SCs) is the existence of topologically protected conducting boundary modes. The recent experimental observation of these edge and surface states in spin-orbit induced $\mathbb{Z}_2$ topological insulators in two and three dimensions,[1] respectively, has lead to a surge of interest and excitement.[2] An exhaustive classification of topologically protected boundary modes occurring in gapped free fermion systems in terms of symmetry and spatial dimension was given in Refs. 3–5. Interestingly, this classification scheme, which is known as the "periodic table" of topological insulators and SCs, predicts a three-dimensional (3D) topological SC which satisfies time-reversal symmetry, but breaks spin-rotation symmetry. Indeed, the B phase of ^{3}He is one example of this so-called "class DIII" topological superfluid, whose different topological sectors can be distinguished by an integer topological invariant. Recent transverse acoustic impedance measurements in ^{3}He-B confirmed the existence of the predicted surface Majorana bound state.[6]

However, finding an electronic analog of the superfluid B phase of ^{3}He remains an outstanding challenge. In this Rapid Communication we argue that some of the 3D noncentrosymmetric SCs might be examples of electronic topological SCs in symmetry class DIII.[7] We analyze the topological phase diagram of these systems and demonstrate quite generally that adjacent to fully gapped topological phases there exist nontrivial gapless superconducting phases with topologically protected nodal lines (rings). To characterize these gapless lines we introduce a set of topological invariants and show that, due to the bulk-boundary correspondence, the presence of topologically stable nodal rings implies the appearance of dispersionless zero-energy Andreev surface states. These topologically protected surface flat bands manifest themselves in scanning tunneling spectroscopy (STS) as a zero bias conductance peak, a feature which could be used as an experimental signature of the topological nontriviality.

In noncentrosymmetric SCs the absence of inversion in the crystal structure generates antisymmetric spin-orbit couplings (SOCs) and leads to a mixing of spin-singlet and spin-triplet pairing states. These are the properties that give rise to topologically nontrivial quasiparticle band structures in these systems. Starting with $CePt_3Si$,[8] a multitude of noncentrosymmetric SCs has recently been discovered, including, among others, $Li_2Pd_xPt_{3-x}B$.[9]

Model Hamiltonian. As a generic phenomenological description applicable to any of the aforementioned materials we employ a single-band model with antisymmetric SOC and treat superconductivity at the mean-field level. Thus, let us consider $\mathcal{H} = \sum_{\boldsymbol{k}} \Psi_{\boldsymbol{k}}^\dagger H(\boldsymbol{k}) \Psi_{\boldsymbol{k}}$ with $\Psi_{\boldsymbol{k}} = (c_{\boldsymbol{k}\uparrow}, c_{\boldsymbol{k}\downarrow}, c_{-\boldsymbol{k}\uparrow}^\dagger, c_{-\boldsymbol{k}\downarrow}^\dagger)^T$, where $c_{\sigma\boldsymbol{k}}^\dagger$ is the electron creation operator with spin σ and momentum $\boldsymbol{k}$ and the Bogoliubov-de Gennes (BdG) Hamiltonian is given by

$$H(\boldsymbol{k}) = \begin{pmatrix} h(\boldsymbol{k}) & \Delta(\boldsymbol{k}) \\ \Delta^\dagger(\boldsymbol{k}) & -h^T(-\boldsymbol{k}) \end{pmatrix}. \tag{1}$$

The normal state Hamiltonian $h(\boldsymbol{k})$ describes noninteracting electrons in a crystal without inversion center $h(\boldsymbol{k}) = \varepsilon_{\boldsymbol{k}}\sigma_0 + \boldsymbol{\gamma}_{\boldsymbol{k}} \cdot \boldsymbol{\sigma}$, where $\varepsilon_{\boldsymbol{k}} = \varepsilon_{-\boldsymbol{k}}$ is the spin-independent part of the spectrum, $\sigma_{1,2,3}$ stand for the three Pauli matrices, and σ_0 denotes the 2×2 unit matrix. The second term in $h(\boldsymbol{k})$ represents an antisymmetric SOC with coupling constant $\boldsymbol{\gamma}_{\boldsymbol{k}}$.

Due to the presence of the parity-breaking SOC $\boldsymbol{\gamma}_{\boldsymbol{k}}$ the order parameter in Eq. (1) is in general an admixture of spin-singlet $\psi_{\boldsymbol{k}}$ and spin-triplet $\boldsymbol{d}_{\boldsymbol{k}}$ pairing states $\Delta(\boldsymbol{k}) = (\psi_{\boldsymbol{k}}\sigma_0 + \boldsymbol{d}_{\boldsymbol{k}} \cdot \boldsymbol{\sigma})(i\sigma_2)$, where $\psi_{\boldsymbol{k}}$ and $\boldsymbol{d}_{\boldsymbol{k}}$ are even and odd functions of $\boldsymbol{k}$, respectively. The direction of the spin-triplet component $\boldsymbol{d}_{\boldsymbol{k}}$ is assumed to be parallel to $\boldsymbol{\gamma}_{\boldsymbol{k}}$, as for this choice the antisymmetric SOC is not destructive for triplet pairing.[10] Hence, we parametrize the $\boldsymbol{d}$ vector and the SOC as $\boldsymbol{d}_{\boldsymbol{k}} = \Delta_t \boldsymbol{l}_{\boldsymbol{k}}$ and $\boldsymbol{\gamma}_{\boldsymbol{k}} = \alpha \boldsymbol{l}_{\boldsymbol{k}}$, respectively. For the spin-singlet component we assume s-wave pairing $\psi_{\boldsymbol{k}} = \Delta_s$ and choose the amplitudes $\Delta_{t,s}$ to be real and positive.

In order to exemplify the topological properties of the BdG Hamiltonian (1), we consider a normal-state tight-binding band structure on the cubic lattice $\varepsilon_{\boldsymbol{k}} = t_1(\cos k_x + \cos k_y + \cos k_z) - \mu$, with hopping amplitude t_1 and chemical potential μ. We will set $(t_1, \mu, \alpha, \Delta_t) = (4.0, 4.8, 1.0, 1.0)$ henceforth. The specific form of the SOC $\boldsymbol{\gamma}_{\boldsymbol{k}}$ depends on the crystal structure,[11] i.e., $g\boldsymbol{\gamma}_{g^{-1}\boldsymbol{k}} = \boldsymbol{\gamma}_{\boldsymbol{k}}$, where g is any symmetry operation in the point group $\mathcal{G}$ of the crystal. Having in mind $Li_2Pd_xPt_{3-x}B$, we assume for the pseudovector $\boldsymbol{l}_{\boldsymbol{k}}$ the

following form compatible with the symmetry requirements of the cubic point group O

$$\boldsymbol{l}_{\boldsymbol{k}} = \begin{pmatrix} \sin k_x \\ \sin k_y \\ \sin k_z \end{pmatrix} - g_2 \begin{pmatrix} \sin k_x(\cos k_y + \cos k_z) \\ \sin k_y(\cos k_x + \cos k_z) \\ \sin k_z(\cos k_x + \cos k_y) \end{pmatrix}, \quad (2)$$

with the constant g_2, and where we neglect higher-order terms. Furthermore, we also consider the point group C_{4v}, relevant for $CePt_3Si$, in which case $\boldsymbol{l}_{\boldsymbol{k}}$ reads

$$\begin{aligned} \boldsymbol{l}_{\boldsymbol{k}} = {} & (\sin k_y \hat{\boldsymbol{e}}_x - \sin k_x \hat{\boldsymbol{e}}_y) \quad (3) \\ & + g_2 \sin k_x \sin k_y \sin k_z (\cos k_x - \cos k_y) \hat{\boldsymbol{e}}_z. \end{aligned}$$

It is important to note that the quasiparticle band topology of $H(\boldsymbol{k})$, as defined by Eq. (1), is mainly determined by the momentum dependence of $\boldsymbol{l}_{\boldsymbol{k}}$ along the Fermi-surface sheets. Hence, the results we obtain are expected to remain qualitatively unchanged upon inclusion of further-neighbor hopping terms in the band structure $\varepsilon_{\boldsymbol{k}}$.

Topological invariants. To characterize the topological properties of $H(\boldsymbol{k})$ we introduce three different topological invariants. But before doing so, we observe that $H(\boldsymbol{k})$ satisfies both time-reversal symmetry (TRS), with $\mathcal{T}^2 = -1$, and particle-hole symmetry (PHS), with $\mathcal{C}^2 = +1$, which are the defining symmetry properties of symmetry class DIII in the terminology of Ref. 3. Combining TRS and PHS yields a third discrete symmetry, the "chiral" symmetry $\mathcal{S} = \mathcal{T}\mathcal{C}$, i.e., there is a unitary matrix $\mathcal{S}$ which anticommutes with $H(\boldsymbol{k})$. It is important to note that while both TRS and PHS relate $H(\boldsymbol{k})$ to $H^T(-\boldsymbol{k})$, $\mathcal{S}$ is a symmetry which is satisfied by $H(\boldsymbol{k})$ at any given point $\boldsymbol{k}$ in the Brillouin zone (BZ).

As shown in Ref. 3 topological sectors in the fully gapped phases of $H(\boldsymbol{k})$ are distinguished by the winding number

$$\nu = \int_{\mathrm{BZ}} \frac{d^3k}{24\pi^2} \varepsilon^{\mu\nu\rho} \operatorname{Tr}[(q^{-1}\partial_\mu q)(q^{-1}\partial_\nu q)(q^{-1}\partial_\rho q)], \quad (4)$$

where the integral is over the first BZ and $q(\boldsymbol{k})$ is the off-diagonal block of the flat-band matrix of $H(\boldsymbol{k})$.[12]

In the nodal superconducting phases the winding number ν is no longer quantized. However, we can consider $H(\boldsymbol{k})$ restricted to 1D loops in reciprocal space and define a topological number in terms of a 1D momentum space loop integral to characterize the topology of the gapless phases. We observe that $H(\boldsymbol{k})$ confined to a generic momentum space loop no longer satisfies TRS nor PHS, but it still obeys chiral symmetry $\mathcal{S}$. Hence, $H(\boldsymbol{k})$ restricted to a loop in the BZ belongs to symmetry class AIII[3] and its topological characteristics are described by the 1D winding number

$$N_{\mathcal{L}} = \frac{1}{2\pi i} \oint_{\mathcal{L}} dl \operatorname{Tr}[q^{-1}(\boldsymbol{k}) \nabla_l q(\boldsymbol{k})], \quad (5)$$

where the integral is evaluated along the loop $\mathcal{L}$ in the BZ. Observe that for *any* closed loop $\mathcal{L}$ that does not intersect with gapless regions in the BZ, $N_{\mathcal{L}}$ is quantized to integer values. If $\mathcal{L}$ is chosen such that it encircles a line node, then $N_{\mathcal{L}}$ determines the topological stability (i.e., the topological charge) of the gapless line.[13,14]

Finally, we also consider $H(\boldsymbol{k})$ restricted to a time-reversal invariant (TRI) loop $\mathcal{L}$, which is mapped onto itself under $\boldsymbol{k} \to -\boldsymbol{k}$. In that case we obtain a 1D Hamiltonian satisfying both TRS and PHS (i.e., belonging to symmetry class DIII). The topological properties of such a 1D system are characterized by the following $\mathbb{Z}_2$ invariant[12]

$$W_{\mathcal{L}} = \prod_{\boldsymbol{K}} \mathrm{Pf}[q^T(\boldsymbol{K})]/\sqrt{\det[q(\boldsymbol{K})]}, \quad (6)$$

where $\boldsymbol{K}$ denotes the two TRI momenta on the loop $\mathcal{L}$ and Pf is the Pfaffian. Note that $W_{\mathcal{L}}$ is either $+1$ or -1 for any TRI loop that does not cross gapless regions in the BZ.

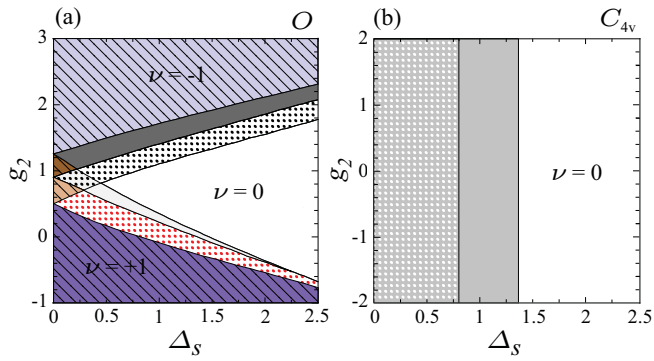

FIG. 1. (Color online) Phase diagram as a function of singlet pairing amplitude Δ_s and SOC g_2 [see Eqs. (2) and (3)] for the point group (a) O and (b) C_{4v}. The gapped phases are characterized by the winding number ν with $\nu = 0$ (white), $\nu = \pm 1$ (dark and light blue hatched), $\nu = -5$ (light brown hatched), and $\nu = +7$ (dark brown hatched). Gray shaded and dotted regions are nodal superconducting phases with $N_{\mathcal{C}_1} = \pm 1$ (red and black dotted), $N_{\mathcal{C}_2} = \pm 1$ (light and dark gray), $N_{\mathcal{C}_3} = +1$ (white dotted), and $N_{\mathcal{C}_4} = +1$ (gray).

Topological phase diagram. Numerical evaluation of the topological numbers (4) and (5) yields the topological phase diagram of $H(\boldsymbol{k})$, which is shown in Fig. 1 as a function of second-order SOC g_2 and relative strength of singlet and triplet pairing components. Fully gapped phases with different topological properties (i.e., the phases labeled by $\nu = \pm 1, 0, -5, +7$) are separated in the phase diagram by regions of nodal superconducting phases (gray shaded and dotted areas). The fully gapped phases with $\nu = \pm 1$ are electronic analogs of ^{3}He-B. The nodal superconducting phases exhibit topologically stable nodal rings, which are centered around high-symmetry axes of the BZ [see Figs. 2(a) and 3(a)]. In order to determine the topological character of these nodal lines (and hence of the corresponding gapless phases) it is sufficient to consider the topological invariant $N_{\mathcal{L}}$ only for loops $\mathcal{L}$ that run along high-symmetry axes. Thus, for the cubic point group O we choose the loops $\mathcal{C}_1 : \Gamma \to M \to X \to \Gamma$ and $\mathcal{C}_2 : \Gamma \to M \to R \to \Gamma$, whereas for the tetragonal point group C_{4v} we consider $\mathcal{C}_3 : \Gamma \to Z \to R \to X \to \Gamma$ and $\mathcal{C}_4 : \Gamma \to Z \to A \to M \to \Gamma$. For the cubic point group we find that whenever $(N_{\mathcal{C}_1}, N_{\mathcal{C}_2}) = (\pm 1, 0)$ there are topologically stable nodal rings centered around the (100) axis (and symmetry-related directions). When $(N_{\mathcal{C}_1}, N_{\mathcal{C}_2}) = (0, \pm 1)$ the gapless lines are oriented along the (111) axis, whereas when $(N_{\mathcal{C}_1}, N_{\mathcal{C}_2}) = (\pm 1, \pm 1)$ the rings are located around the (110) direction. (A similar analysis also holds for the group C_{4v}.)

Andreev surface states. A nonzero quantized value of any of the three topological numbers (4)–(6) implies the existence of zero-energy Andreev surface states. First of all, in fully

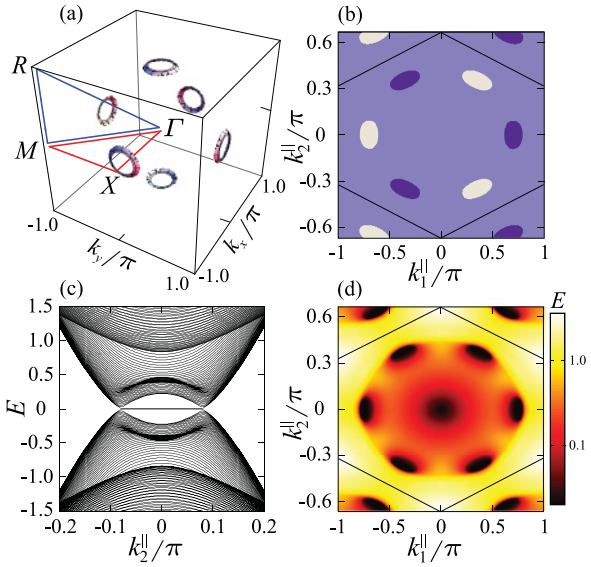

FIG. 2. (Color online) Nodal rings (a) and (111) surface states (c),(d) for the point group O with $(g_2,\Delta_s) = (0.3,0.5)$. This parameter choice corresponds to the red dotted region in Fig. 1(a). (b) Topological invariant $N_{(111)}$, Eq. (7), as a function of surface momentum $\boldsymbol{k}_\parallel$. Gray and dark blue indicate $N_{(111)} = \pm 1$, while light blue is $N_{(111)} = 0$. (c) Band structure for a slab with (111) face as a function of surface momentum $k_2^\parallel$ with $k_1^\parallel = 0.75\pi$. (d) Energy dispersion of the lowest-lying state with positive energy. The color scale is such that black corresponds to zero energy. The states at zero energy in (c) and (d) are localized at the surface. The flat bands in (c) and (d) are singly degenerate (i.e., one branch per surface), whereas the linearly dispersing zero mode at the center of the BZ in (d) is doubly degenerate.

gapped phases with topologically nontrivial character there appear linearly dispersing Majorana surface modes.[3,15–17] In order to understand the appearance of zero-energy Andreev surface states in the gapless phases, we now make use of the topological invariant $N_{\mathcal{L}}$ with a cleverly chosen loop $\mathcal{L}$. Let us consider Eq. (1) in a slab configuration with (lmn) face.

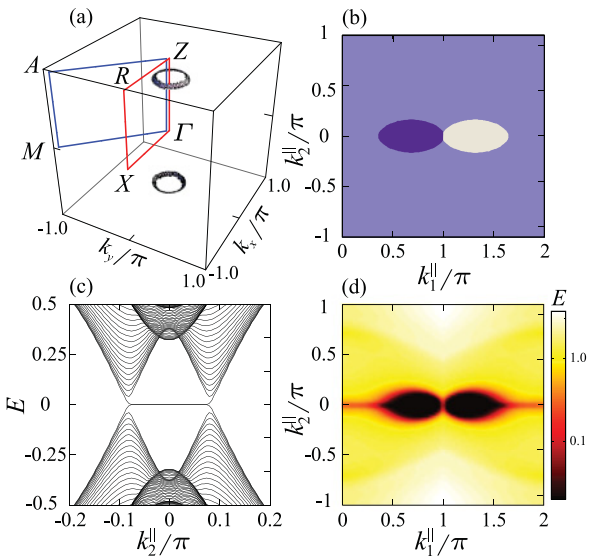

FIG. 3. (Color online) Same as Fig. 2 but for the point group C_{4v}, for a slab with (012) face, and with $(g_2,\Delta_s) = (0.0,0.5)$. This parameter choice corresponds to the white dotted area in Fig. 1(b).

In this geometry the Hamiltonian $H_{(lmn)}$ retains translational invariance along the two independent directions parallel to the (lmn) surface. Hence, $H_{(lmn)}(\boldsymbol{k}_\parallel)$ can be viewed as a family of 1D systems parametrized by the two surface momenta $\boldsymbol{k}_\parallel = (k_1^\parallel, k_2^\parallel)$. Since $H_{(lmn)}(\boldsymbol{k}_\parallel)$ obeys chiral symmetry (but breaks in general TRS and PHS), its topological properties are given by the 1D winding number of class AIII

$$N_{(lmn)}(\boldsymbol{k}_\parallel) = \frac{1}{2\pi i}\int dk_\perp \,\mathrm{Tr}[q^{-1}(\boldsymbol{k})\partial_\perp q(\boldsymbol{k})], \qquad (7)$$

where $k_\perp$ is the bulk momentum perpendicular to the surface, and $\partial_\perp = \partial/\partial k_\perp$. Note that $N_{(lmn)}$ is the same as $N_{\mathcal{L}}$, Eq. (5), with $\mathcal{L}$ chosen along $k_\perp$, following a noncontractible cycle of the BZ torus T^3.

Now, the key observation is that the above line integral is closely related the loop integral $N_{\mathcal{L}}$, with $\mathcal{L} = \mathcal{C}_i$, that determines the topological charge of the superconducting nodal lines. That is, for those surface momenta $\boldsymbol{k}_\parallel$ for which the loop along $k_\perp$ in Eq. (5) passes through just one nontrivial nodal ring, $N_{(lmn)}(\boldsymbol{k}_\parallel)$ is equal to the topological charge of this given nodal ring. Hence, if we plot $N_{(lmn)}(\boldsymbol{k}_\parallel)$ as a function of surface momenta [see Figs. 2(b) and 3(b)], we find that the boundaries separating regions with different winding number are identical to the projection of the nodal lines onto the (lmn) plane. Furthermore, since a nonzero quantized value of $N_{(lmn)}$ implies the existence of zero-energy states at the end points of the 1D Hamiltonian $H_{(lmn)}(\boldsymbol{k}_\parallel)$,[3,18] we find that there are zero-energy Andreev bound states on the (lmn) surface located within the projected nodal rings. This conclusion is corroborated by numerical computations of the zero-energy surface states both for the point group O and C_{4v} (see Figs. 2 and 3). When two nodal rings overlap in the (lmn) projection of the BZ, then the quantized value of $N_{(lmn)}$ in the overlapping region is determined by the additive contribution of the topological charges of the two rings. In particular, one can have a situation where the two contributions cancel, in which case there is no zero-energy surface state within the overlapping region.

Finally, using an analogous argument as in the previous paragraph, we can also employ the $\mathbb{Z}_2$ number (6) to deduce the presence of zero energy modes at TRI momenta of the surface BZ.[12] One example of this is the Kramers pair of surface zero modes located at the center of the surface BZ in Fig. 2 (d) (cf. Refs. 16 and 17). Remarkably, this is a surface Majorana mode in a *gapless* (nodal) superconducting phase.[19]

Experimental signatures. One of the most direct signatures of the topological aspects of noncentrosymmetric SCs are the surface Andreev bound states. These can be probed by angle-resolved photoemission measurements, or by STS of the surface density of states (SDOS). STS has proved to be an effective tool to explore surface states of two-dimensional unconventional superconductors, see, e.g., Refs. 20–24. The bulk density of states of 3D gapless SCs with nodal lines vanishes linearly at zero energy. In contrast, the surface flat bands lead to a diverging zero-energy peak in the SDOS (see Fig. 4).

The zero-bias peak in the SDOS is strongly dependent on the surface orientation. From this dependence it is in principle possible to (partially) map out the location of the topologically stable nodal lines in the bulk BZ. In addition, one can take advantage of the fact that an applied magnetic field leads to a splitting of the zero-energy peak. Again, this splitting is

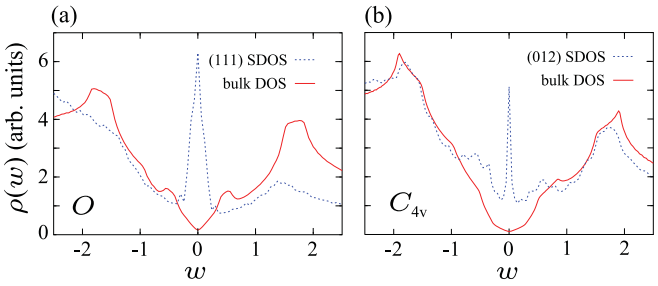

FIG. 4. (Color online) Surface and bulk density of states for the point group (a) O and (b) C_{4v}. The surfaces are oriented perpendicular to the (111) and (012) axes, respectively. The employed parameter values are the same as in Figs. 2 and 3.

strongly dependent on the orientation of the magnetic field axis with respect to the nodal lines. Another possibility is to use spatially resolved STS to investigate the SDOS in the presence of impurities on the surface. It is expected that surface impurities will lead to strong spatial modulations of the SDOS, which might give some information about the topological characteristics of the nodal lines in the bulk.

Stability of surface modes. The zero-energy surface flat bands in time-reversal symmetric noncentrosymmetric SCs are topologically protected against the opening of a gap and are therefore stable against weak symmetry preserving deformations. Conversely, any perturbation that leads to a gap opening of the surface states is expected to be accompanied by the breaking of the symmetries of the time-reversal symmetric SC, i.e., TRS or certain types of translational invariance. One possible scenario, for example, is that interactions might lead to spontaneous TRS breaking at the boundary of the SC, such as to the coexistence of TRS breaking and TRS preserving order parameters near the surface. This would be observable in experiments, for instance, as a splitting of the zero-bias conductance peak.

In conclusion, using three different topological invariants, we examined the topological properties of general 3D noncentrosymmetric superconductors with TRS. We showed that in nodal superconducting phases there always appear dispersionless Andreev surface bands. We established a correspondence between these zero-energy surface flat bands and the topologically protected nodal lines in the bulk, thereby revealing the topological origin of the surface flat band. In particular, we demonstrated that the projection of the nodal lines on the surface coincides with the boundary of the surface flat band. We emphasize that the presented formalism (or a generalization thereof) can be applied to any 3D unconventional SC that preserves TRS. One particularly interesting family of compounds is $Li_2Pd_xPt_{3-x}B$. In these SCs the substitution of Pd by Pt seems to be related to the relative strength of singlet and triplet pairing states.[25] Hence, it might be possible to observe in $Li_2Pd_xPt_{3-x}B$ the transition between two topologically distinct quantum phases as a function of Pt concentration.

The authors thank B. Béri, A. Furusaki, L. Klam, A. Ludwig, R. Nakai, P. Horsch, and M. Sigrist for discussions. A.P.S. is grateful to the Aspen Center for Physics for hospitality during the preparation of this work. S.R. is supported by Center for Condensed Matter Theory at UCB.

[1] M. König, S. Wiedmann, C. Brüne, A. Roth, H. Buhmann, L. W. Molenkamp, X-L. Qi, and S-C. Zhang, Science **318**, 766 (2007); D. Hsieh, D. Qian, L. Wray, Y. Xia, Y. Hor, R. Cava, and M. Hasan, Nature (London) **452**, 970 (2008).

[2] M. Z. Hasan and C. L. Kane, Rev. Mod. Phys. **82**, 3045 (2010); X.-L. Qi and S.-C. Zhang, e-print arXiv:1008.2026.

[3] A. P. Schnyder, S. Ryu, A. Furusaki, and A. W. W. Ludwig, Phys. Rev. B **78**, 195125 (2008); in *Advances in Theoretical Physics*, edited by Vladimir Lebedev and Mikhail Feigel'man, AIP Conf. Proc. No. 1134 (AIP, Melville, NY, 2009), p. 10.

[4] A. Y. Kitaev, in *Advances in Theoretical Physics*, edited by Vladimir Lebedev and Mikhail Feigel'man, AIP Conf. Proc. No. 1134 (AIP, Melville, NY, 2009), p. 22.

[5] S. Ryu, A. P. Schnyder, A. Furusaki, and A. W. W. Ludwig, New J. Phys. **12**, 065010 (2010).

[6] S. Murakawa, Y. Tamura, Y. Wada, M. Wasai, M. Saitoh, Y. Aoki, R. Nomura, Y. Okuda, Y. Nagato, M. Yamamoto, S. Higashitani, and K. Nagai, Phys. Rev. Lett. **103**, 155301 (2009).

[7] Topological SCs in class DIII may also be found among *centrosymmetric* SCs with triplet pairing, see, e.g., G. E. Volovik and L. P. Gorkov, Sov. Phys. JETP **61**, 843 (1985).

[8] E. Bauer, G. Hilscher, H. Michor, Ch. Paul, E. W. Scheidt, A. Gribanov, Yu. Seropegin, H. Noël, M. Sigrist, and P. Rogl, Phys. Rev. Lett. **92**, 027003 (2004).

[9] K. Togano, P. Badica, Y. Nakamori, S. Orimo, H. Takeya, and K. Hirata, Phys. Rev. Lett. **93**, 247004 (2004); P. Badica, T. Kondo, and K. Togano, J. Phys. Soc. Jpn. **74**, 1014 (2005).

[10] P. A. Frigeri, D. F. Agterberg, A. Koga, and M. Sigrist, Phys. Rev. Lett. **92**, 097001 (2004).

[11] K. V. Samokhin, Ann. Phys. **324**, 2385 (2009).

[12] See Supplemental Material at http://link.aps.org/supplemental/10.1103/PhysRevB.84.060504 for details of the calculation.

[13] B. Béri, Phys. Rev. B **81**, 134515 (2010).

[14] M. Sato, Phys. Rev. B **73**, 214502 (2006).

[15] X.-L. Qi, T. L. Hughes, S. Raghu, and S-C. Zhang, Phys. Rev. Lett. **102**, 187001 (2009).

[16] A. B. Vorontsov, I. Vekhter, and M. Eschrig, Phys. Rev. Lett. **101**, 127003 (2008).

[17] M. Eschrig, C. Iniotakis, and Y. Tanaka, e-print arXiv:1001.2486.

[18] S. Ryu and Y. Hatsugai, Phys. Rev. Lett. **89**, 077002 (2002).

[19] For a similar majorana Andreev state at edges of 2D nodal superconductors, see M. Sato and S. Fujimoto, Phys. Rev. Lett. **105**, 217001 (2010).

[20] Y. Tanaka and S. Kashiwaya, Phys. Rev. Lett. **74**, 3451 (1995).

[21] S. Kashiwaya and Y. Tanaka, Rep. Prog. Phys. **63**, 164 (2000).

[22] Y. Tanaka, Y. Mizuno, T. Yokoyama, K. Yada, and M. Sato, Phys. Rev. Lett. **105**, 097002 (2010).

[23] K. Yada, M. Sato, Y. Tanaka, and T. Yokoyama, Phys. Rev. B **83**, 064505 (2011).

[24] M. Sato, Y. Tanaka, K. Yada, and T. Yokoyama, Phys. Rev. B **83**, 224511 (2011).

[25] H. Q. Yuan, D. F. Agterberg, N. Hayashi, P. Badica, D. Vandervelde, K. Togano, M. Sigrist, and M. B. Salamon, Phys. Rev. Lett. **97**, 017006 (2006).